Title: Drug-tolerant idling melanoma cells exhibit theory-predicted metabolic low-low phenotype

Authors/Affiliations:
Dongya Jia[1,*], B. Bishal Paudel[2,3,4,*], Corey E. Hayford[2,3,5], Keisha N. Hardeman[2,3], Herbert Levine[1,6,7,#], Jose Onuchic[1,8,9,10,#] and Vito Quaranta[2,3,#]
[1]Center for Theoretical Biological Physics, Rice University, Houston, TX 77005;
[2]Department of Biochemistry, Vanderbilt University, Nashville, TN 37232;
[3]Quantitative Systems Biology Center (QSBC), Vanderbilt University, Nashville, TN 37232;
[4]Department of Biomedical Engineering, University of Virginia, Charlottesville, VA 22908;
[5]Chemical and Physical Biology Graduate Program, Vanderbilt University, Nashville, TN 37232;
[6]Department of Bioengineering, Northeastern University, Boston, MA 02115, USA
[7]Department of Physics, Northeastern University, Boston, MA 02115, USA
[8]Department of Biosciences, Rice University, Houston, TX 77005;
[9]Department of Physics and Astronomy, Rice University, Houston, TX 77005;
[10]Department of Chemistry, Rice University, Houston, TX 77005;

*These authors contributed equally.
[#]These authors contributed equally.

Address Correspondence to:
Vito Quaranta (vito.quaranta@vanderbilt.edu)
Herbert Levine (h.levine@northeastern.edu)
Jose Onuchic (jonuchic@rice.edu)

Abstract (max. words: 150)

Cancer cells adjust their metabolic profiles to evade treatment. Metabolic adaptation is complex and hence better understood by an integrated theoretical-experimental approach. Using a minimal kinetic model, we predicted a previously undescribed Low/Low phenotype, characterized by low oxidative phosphorylation (OXPHOS) and low glycolysis. Here, we report that L/L metabolism is observed in *BRAF*-mutated melanoma cells that enter a drug-tolerant "idling state" upon long-term MAPK inhibition (MAPKi). Consistently, using publicly available RNA-sequencing data of both cell lines and patient samples, we show that melanoma cells decrease their glycolysis and/or OXPHOS activity upon MAPKi and converge toward the L/L phenotype. L/L metabolism is unfavorable for tumor growth, yet supports successful cell division at ~50% rate. Thus, L/L drug-tolerant idling cells are a reservoir for accumulating mutations responsible for relapse, and should be considered as a target subpopulation for improving MAPKi outcomes in melanoma treatment. (*word count: 148*)

Statement of Significance (max. Words: 50):

Tumor relapse is almost universal during drug treatment of melanoma patients. Theory coupled with experimentation has uncovered a previously undescribed metabolically inactive state in melanoma upon MAPKi treatment, pointing to novel strategies to prevent relapse. (*word count: 35*)

Introduction:

Cancer cells can adapt their metabolic profiles to survive drug treatment. Traditionally, the Warburg effect or aerobic glycolysis was regarded as the dominant metabolic phenotype in cancer (1). Recently, mitochondrial OXPHOS has been shown to also play a critical role, especially during metastasis and drug-resistance (2). Accumulating evidence suggests that cancer cells, in response to external perturbations, can adapt their metabolic profiles by utilizing glycolysis, OXPHOS, or both, referred to as metabolic plasticity (3). For instance, melanoma cells upon BRAF inhibition (BRAFi) can exhibit enhanced OXPHOS (4,5). We and others (6,7) have shown that BRAFi is most effective when melanoma cells rely primarily on glycolysis (or forced to utilize glycolysis by depleting mitochondria). Drug-tolerant cancer cells have been shown to have increased dependency on certain substrates such as glutamine (5) and polyunsaturated lipids (8). Taken together, these results underscore a critical role of metabolic adaptation in cancer cell survival.

To elucidate metabolic plasticity in cancer, we established a modeling framework that couples gene regulation with metabolic pathways (***Supplementary Fig. S1***) (3). Our modeling analysis demonstrates a direct association of the master gene regulators of cancer metabolism AMP-activated protein kinase (AMPK) and hypoxia-inducible factor (HIF)-1 with three major metabolic pathways - glycolysis, glucose oxidation and fatty acid oxidation (FAO). Specifically, the model predicts the existence of a hybrid metabolic state where cancer cells can use both glycolysis and OXPHOS, and a metabolically inactive state where cancer cells exhibit low activity of both glycolysis and OXPHOS, referred to as the “low/low” (L/L) state. The importance of this new state has to date remained uncertain.

It is well-established that bacterial populations can harbor a subpopulation of persister states that exhibit tolerance to antibiotics (9). Interestingly, persisters seem to have altered metabolism as compared to the drug sensitive cells. Similar to bacterial persisters, several possible forms of drug ‘persisters’ have been described in cancer, including quiescent (10), senescent (11),

dormant (12) and drug-tolerant cells (13). Recently, we reported that *BRAF*-mutated melanoma cells converge toward a non-quiescent "idling population state" upon long-term MAPKi treatment (14). In a sense, the idling state defines a form of drug-tolerance since the total cell population does not expand; rather, it is maintained at a constant size (i.e. it idles) by undergoing cell division and death at approximately equal rates within clonal lineages of single-cell derived subclones. Nonetheless, each round of successful cell division brings with it the possibility of accumulating mutations, a gateway to acquired drug resistance under drug selective pressure, and concomitant relapse.

Inspired by the theoretical predictions and the analogy to bacterial persisters, we investigated the possibility that the L/L phenotype could characterize the drug-tolerant idling state. Here, we report that the SKMEL5 melanoma cells can indeed repress both their glycolysis and OXPHOS activity when they transition into the idling state as a response to therapy. Furthermore, using the RNA-sequencing (RNA-Seq) data of human melanoma M397 and M229 cell lines and melanoma patient samples from from Gene Expression Omnibus (GEO), we show that melanoma cells consistently decrease their glycolysis and/or OXPHOS activity and exhibit a convergence toward the L/L phenotype upon long-term MAPKi treatment, as characterized by the AMPK/HIF-1 signatures (15) and the metabolic pathway scores (3). The residual melanoma tumors may be composed of a significant fraction of drug-tolerant idling cells. We further use the mathematical model to explore conditions that promote the L/L phenotype and show that high HIF-1 degradation or low mtROS production can significantly enhance the L/L phenotype. In summary, the L/L metabolic phenotype, predicted by mathematical modeling and validated by experiments, can be a potential bottleneck for melanoma treatment.

Results:

Modeling-Predicted Metabolically L/L Phenotype in Cancer

We previously developed a metabolic modeling framework that couples the regulatory circuit AMPK:HIF-1:ROS with three major metabolic pathways - glycolysis, glucose oxidation and FAO (***Supplementary Fig. S1***). The outputs of the model are the stable steady-state levels of phosphorylated AMPK (pAMPK), the active form of AMPK, HIF-1 (H), mtROS (R_{mt}), noxROS (R_{nox}) and the rates of glucose oxidation (G1), glycolysis (G2) and FAO (F). Using the modeling framework, we show that cancer cells can robustly acquire four stable metabolic states "O", "W", "W/O" and "L/L" corresponding to an OXPHOS phenotype, a glycolysis phenotype, a hybrid metabolic phenotype, and a metabolically inactive low/low phenotype respectively (***Figs. 1A-C***).

The “O” state is characterized by high AMPK activity and high OXPHOS pathway activity. The “W” state is characterized by both high HIF-1 activity and high glycolysis pathway activity. The “W/O” state is characterized by high AMPK/HIF-1 activity and high OXPHOS/glycolysis pathway activity. The “L/L” state is characterized by low AMPK/HIF-1 activity and low OXPHOS/glycolysis pathway activity (***Fig. 1C***). The existence of this “L/L” state has until now remained an unverified prediction. Notably, the fractional occurrences of “W” and “O” states within our model are often much larger than those of “W/O” and “L/L” states, indicating the emergence of “W/O” and “L/L” states probably requires specific modifications to the parameters of the baseline cellular network.

To study how cellular network changes its dynamics under parameter perturbations, we focus on two factors: HIF-1 degradation and mtROS production. These two factors are chosen as cancer cells often face varying hypoxic conditions (16), and also undergo changes in their mitochondria (2). Previously, we showed that stabilized HIF-1 or elevated production of mtROS promotes the “W/O” state. Here, we focused on their effects on the acquisition of the “L/L” state. To investigate the emergence of the “L/L” state, we considered four scenarios - (high mtROS, high HIF-1), (high mtROS, low HIF-1), (low mtROS, high HIF-1) and (low mtROS, low HIF-1). We utilize a previously developed computation method called RAndom CIrcuit PErturbation (RACIPE) (17) to identify the robust metabolic states resulting from each scenario. Specifically, we randomly sampled values for each parameter from the range ($75\%P_0$, $125\%P_0$) where P_0 is the baseline value; this was done for all parameters except for the degradation rate of HIF-1 and production rate of mtROS, which are fixed so as to distinguish among the different scenarios. We construct 500 sets of randomly sampled parameters, calculate the stable steady-state solutions for each set of parameters, and collect solutions from all sets of parameters for statistical analysis by which the dominant metabolic profiles can be identified. We find that the fraction of the “L/L” metabolic state is lowest when both the HIF-1 level and the mtROS level are high (***Fig. 1D i, Supplementary Fig. S2 i***), intermediate when either HIF-1 or mtROS are high (***Figs. 1D-E ii-iii, Supplementary Fig. S2 ii -iii***), and highest when both the HIF-1 level and the mtROS level are low (***Fig. 1D iv, Supplementary Fig. S2 iv***). In summary, our modeling analysis shows that cancer cells can exist in four distinct metabolic states and the occupancies of different metabolic states can be altered by specific kinetic paramter modifications. Specifically, we show that the metabolically L/L state is enriched when the degradation rate of HIF-1 is high or the production rate of mtROS is low.

Idling Melanoma Cells Exhibit the Metabolic L/L Characteristics

We recently reported that *BRAF*-mutated SKMEL5 melanoma cells enter a non-quiescent "idling" population state upon long-term MAPKi treatment (14). Briefly, melanoma cells, including isogenic single-cell derived subclones (SC01, SC07, SC10), exhibit an early differential drug response before transitioning into an idling state characterized by ~zero net-growth (14). In particular, SC01 and SC10 had divergent initial response to BRAFi (negative for SC01, positive for SC10), but both subclones exhibit ~zero net-growth rates under continued exposure to MAPKi, while SC07 maintained its initial ~zero net-growth (***Fig. 2A***). At the population level, the idling state exhibits stable population size, realized by an approximately equal rates of division and death (14). Since recent studies show that melanoma cells treated with MAPKi undergo metabolic reprogramming (4,18), we seek to characterize the metabolic profiles of isogenic subclones at baseline and *en route* to the idling state.

To characterize the change of metabolic activity in single-cell derived subclones upon treatment, we apply the previously developed AMPK/HIF-1 signatures and and metabolic pathway scores to quantify the activity of AMPK and HIF-1, and the activity of three major metabolic processes - the citric acid cycle (TCA), FAO and glycolysis. Strikingly, by applying these signatures to the longitudinal RNA-Seq data of the isogenic subclones upon BRAFi at baseline (0d), day 3 (3d) and at day 8 (8d, idling state), we find the subclone SC01 exhibit lowest AMPK/HIF-1 activity and lowest TCA/FAO/glycolysis activity (***Figs. 2B-C***, ***Supplementary Fig. S3***). Upon MAPKi treatment, we find that the melanoma cells increase both their AMPK and HIF-1 activities from baseline to day 3 and then decrease both from day 3 to day 8, with an overall decrease from day 0 to day 8, especially for the subclones SC01 and SC10 (***Fig. 2B, Supplementary Fig. S3***). The subclone SC07 decreases its AMPK activity while increasing its HIF-1 activity from baseline to day 3 to day 8 (***Fig. 2B, Supplementary Fig. S3).*** The TCA/FAO activity for both SC01 and SC10 initially increases and then decreases from day 3 to day 8, with an overall decrease from day 0 to day 8. The glycolysis activity of both SC01 and SC10 decreases from its baseline to day 8.(***Fig. 2C***). Interestingly, the TCA/FAO activity of SC07 decrease from its baseline to day 8. (***Fig. 2C***), In the only outlier, the glycolysis score of SC07 first decreases, and then slightly increases. Nonetheless, taken all together our analysis suggests that change in central metabolism has a critical role in drug response.

To further test whether the convergence to the L/L state is a common trend of melanoma cells upon long-term treatment, we apply the AMPK/HIF-1 signatures and the metabolic pathway

scores to quantify the change of metabolic profiles of two *BRAF*-mutated melanoma cell lines, M397 and M229 upon vemurafenib treatment for up to three months (19). Our analyses show that while the M397 and M229 cells have different initial AMPK and HIF-1 activities, both exhibit a significant decrease in their AMPK and/or HIF-1 activities in response to vemurafenib within 21 days (***Supplementary Fig. S4A***). Interestingly, the M229 cells increase its AMPK activity after day 21 and recover its AMPK activity comparable to its baseline at day 90 (***Supplementary Fig. S4A***). In both cell lines, the TCA and glycolysis scores decrease during the course of the treatment while the FAO score does not show a clear difference from its baseline (***Supplementary Fig. S4B***), In summary, the M397 and M229 cells exhibit the L/L gene signatures upon vemurafenib treatment.

To directly test the modeling-predicted and metabolic signatures-characterized L/L state, we measure the metabolic activity of cells in the idling state relative to cells at baseline. We quantify both the oxygen consumption rate (OCR) and extracellular acidification rate (ECAR) (*see* ***Materials and Methods***) in isogenic subclones using the Seahorse extracellular flux analyzer platform (Agilent). At baseline, the OCRs are different in different subclones - SC07 (*highest*), SC10 (*intermediate*) and SC01 (*lowest*). In the idling state, we find that the OCR of both SC07 and SC10 are significantly reduced, while SC01 exhibited little change from its already low initial OCR (***Fig. 2D, top panel***), which is consistent with the characterization results by the metabolic pathway scores (***Fig. 2C***). Similar results are obtained for ECAR (***Fig. 2D, bottom***). From the metabolic parameters extracted from Seahorse assays as previously described (6), we aggregate the glycolysis-related and OXPHOS-related parameters (***Fig. 2E***), and project subclones at baseline and in idling state into two-dimensional metabolic space. Consistent with earlier results (***Figs. 2C-D***), SC10 exhibits a significant reduction in both its glycolytic and its OXPHOS profile, while SC01 exhibits relatively little change from its already low baseline (***Fig. 2E***). To examine the temporal evolution to the idling state, we perform principal component analysis (PCA) on the RNA-Seq data of the genes related to metabolism based on the Molecular Signatures Database (MSigDB) for all three subclones (***Supplementary Table S1***). Interestingly, metabolic gene expression profiles of all three subclones converge in both the principal components 1 and 2 (PC1 & PC2) when entering the idling state (***Fig. 2G***). Taken together, these results suggest that the *BRAF*-mutated melanoma cells, including the isogenic subclones, under MAPKi treatment, tend to decrease both their glycolysis and OXPHOS activities and acquire a L/L state, while converging to an idling state. The L/L state thus

appears to be a common feature of idling melanoma cells, that could also explain a recently described treatment-induced dedifferentiation in melanoma cells (19).

Residual Melanoma Tumors on MAPKi Therapy Display the Metabolically L/L Signature

The modeling-predicted and experiment-validated metabolically-inactive L/L state of idling melanoma cells motivates us to further analyze whether such a L/L phenotype can be observed in melanoma patient samples. We analyze the change of the metabolic activity in a cohort of melanoma patients before and during MAPKi treatment (20). Strikingly, even though there are only 7 patients, we observe a consistent temporal decrease of both AMPK and HIF-1 activity upon MAPKi treatment in 6 of the 7 patients (***Fig. 3***). Additionally, using the metabolic pathway scores, we observe that the samples that underwent longer treatment (patients 1, 3 and 4) exhibit a decrease of both glycolysis and TCA scores (Fig. 3 left panel), while the samples with shorter treatment (patients 6, 7 and 8) exhibit a decrease in glycolysis score (Fig. 3 right panel). Patient 2, however, shows a decrease in HIF-1 activity and an increase in AMPK activity (***Supplementary Fig. S5A***). In contrast, the FAO score increases upon treatment in almost all patients (***Supplementary Fig. S5B***), which suggests that the drug-tolerant cells tend to depend on lipid metabolism as reported before (19).

We also obtain the RNA-Seq data of melanoma patient samples from The Cancer Genome Atlas (TCGA) and evaluate their AMPK/HIF-1 activity. We find that the melanoma patient samples can be grouped into four clusters based on their HIF-1 and AMPK signatures (***Supplementary Fig. S6***). In addition to patient samples that exhibit either high HIF-1 activity (corresponding to a glycolysis state) or high AMPK activity (corresponding to an OXPHOS state), high activity of both HIF-1 and AMPK (corresponding to a hybrid metabolic state), there exists a fraction of samples that show low activity of both HIF-1 and AMPK, tentatively characterized as the L/L state (***Supplementary Fig. S6***). Consistent with the cell line data, the HIF-1 and AMPK activities of melanoma samples are different at baseline among patients. Interestingly, in almost all cases, there is a decrease in their activities upon treatment (***Supplementary Fig. S5C***), indicating a significant trend towards the L/L state.

Discussion:

Drug-tolerance remains a challenge in anti-cancer therapies. In recent years, metabolic plasticity has sometimes been linked to drug-tolerance. However, it remains largely unknown how cancer cells adjust their metabolic profiles to evade treatment. Through coupling gene

regulation with metabolic pathways, our mathematical model characterizes distinct metabolic states in cancer cells (3). In particular, our model predicts the existence of a metabolically inactive phenotype L/L characterized by low AMPK/HIF-1 activity and low OXPHOS/glycolysis pathway activity. Although metabolic adaptation has been reported in different cancer types (2,4,5,8,21–23), such a L/L metabolic phenotype has not been previously described.

The recently reported idling state acquired by melanoma cells upon long-term MAPKi treatment (14) represents a novel drug-tolerant mechanism that interferes with successful treatment. In the present study, we show that these idling melanoma cells exhibit the predicted L/L phenotype characterized by low AMPK/HIF-1 activity and low OXPHOS/glycolysis pathway activity. We further show that melanoma cells tend to decrease their AMPK/HIF-1 activity and TCA/glycolysis activity upon MAPKi treatment and converge toward a L/L phenotype, through analyzing the RNA-Seq data of both cell lines and patient samples obtained from GEO. Taken together, our results suggest that the acquisition of a L/L state tends to be a general trend for melanoma cells upon long-term MAPKi treatment.

It is worth noting that the acquisition of a L/L phenotype by melanoma cells upon long-term MAPKi treatment is not always direct. Our results suggest that the paths to a L/L phenotype can vary. While the subclones SC01 and SC10 show an initial increase of both their AMPK/HIF-1 and TCA/FAO activities before converging to the L/L phenotype upon the MAPKi treatment, the subclone SC07 continuously decreases its AMPK and TCA/FAO activities. Similarly, in the clinical context, not all patient samples continuously decrease their glycolysis and OXPHOS activity upon treatment. 6 out of 7 patients did show a decrease in both HIF-1 and AMPK activity; one remaining sample (Patient 2) shows a decrease only in its HIF-1 activity. Notably, the melanoma samples from patient 1, 3 and 4 exhibit more pronounced decrease in both their AMPK/HIF-1 activity and TCA/glycolysis activity upon treatment relative to the samples from patient 6, 7 and 8. One possible explanation is that the samples from patient 1, 3 and 4 were obtained upon longer treatment (85 days, 22 days and 267 days respectively) relative to the samples from patients 6, 7 and 8 (15 days, 15 days and 22 days respectively) (***Fig. 3***), as the acquisition of a L/L state may require a long-term treatment. In addition, the differences in treatment regimens may play a role in the acquisition of the L/L phenotype. Interestingly, the FAO scores of samples from patients 3, 4, 7, 8 exhibit a consistent increases upon treatment, which is consistent with the report that these cells exhibit increased dependence on lipid peroxidation pathways, and hence vulnerable to ferroptosis-inducing drugs (19). Therefore, it is

critical to consider the dynamics of cellular response. Indeed, recent reports suggest that an increase in OXPHOS under perturbations in cancer cells (4,5,13,24) might rather be an intermediate response, but not a final stable state, as melanoma cells have been shown to undergo drug-induced dedifferentiation (19).

As the L/L phenotype potentially allows for tumor relapse, it is critical to identify the conditions that promote its existence and enrichment. Using our metabolic modeling framework, we show that high degradation rate of HIF-1 and/or low production rate of mtROS can significantly enhance the L/L phenotype. This is consistent with recent reports that show BRAFi treatment induces degradation of HIF-1α at both mRNA and protein levels in drug-tolerant *BRAF*-mutated melanoma cells (7,23). Additional experimental work to characterize the change of HIF-1 and mtROS in idling cells relative to non-idling cells needs to be done to test this prediction.

The L/L phenotype is potentially observed in a fraction of patient samples that exhibit low activity of both AMPK and HIF-1. Since treatment information regarding patient samples in TCGA is incomplete, it is hard to evaluate the effect of treatment on the acquisition of the L/L phenotype. We speculate that the L/L phenotype enables cancer cells to maintain cell viability and, because of the ongoing cell division, to accumulate mutations *en route* to resistance. One could also speculate that repression of central-carbon metabolism (i.e., decreased glycolysis and OXPHOS activity), as we see in the idling cells, allows cells to synthesize biomolecules to maintain cellular homeostasis (11). This is consistent with recent reports which suggest that drug-tolerant cancer cells exhibit an increased dependence on polyunsaturated lipids for survival (8). The AMPK/HIF-1 signatures and metabolic pathway scores can not only capture the trajectory of treatment-induced metabolic changes but also delineate the differences among different cells and different patient samples. Therefore, the AMPK/HIF-1 signatures may be used to further explore the existence of a L/L phenotype in other types of cancer. This will eventually lead to the understanding of how L/L phenotype could be exploited therapeutically.

Abnormal metabolism has been observed in cancer for over a century. For quite some time, aerobic glycolysis was regarded as the dominant metabolic phenotype. It was hypothesized that the elevated glycolytic activity in cancer was due to the defects in mitochondria. Recently, it has been recognized that cancer mitochondria are not in general dysfunctional but instead they are actively functioning in certain cancer types. By performing systems biology analysis of cancer metabolism, we show that cells are able to acquire a hybrid metabolic phenotype, and a

metabolically L/L phenotype in addition to glycolysis and OXPHOS. From the Warburg effect, to OXPHOS, to hybrid, and now to the L/L phenotype, we are getting closer to a complete picture of the possible metabolic states acquired by cancer cells and how cancer cells adjust their metabolic profiles under perturbations. Since recent efforts in targeting cancer metabolism have been largely ineffective, a better understanding of cancer metabolic plasticity would eventually contribute to more effective therapeutic strategies. We foresee the integration of computational and experimental approaches will be necessary to elucidate mechanisms underlying cancer cell behaviors. Therefore, future studies aimed at limiting metabolic plasticity, metabolic reverse engineering, may provide insights into novel therapeutic regimens.

Acknowledgments:

This work is supported by the National Science Foundation (NSF) grant for the Center for Theoretical Biological Physics NSF PHY-1427654 (to J.N.O. and H.L.), US National Institutes of Health Grants U54 CA217450, U01 CA215845, R01 CA186193, and U01 CA174706 (to V.Q.), Vanderbilt Institute for Clinical and Translational Research (VICTR) grants 16721, and 16721.1 (to B.B.P). J.N.O. is a Cancer Prevention and Research Institute of Texas (CPRIT) Scholar in Cancer Research. D.J. is supported by a training fellowship from the Gulf Coast Consortia, via the Computational Cancer Biology Training Program (CPRIT Grant No. RP170593). We would like to thank Prof. Kevin Janes (University of Virginia) for critical reviews of the manuscript.

Author Contributions:

Conceptualization: D.J., B.B.P.;
Data Acquisition, Analysis, and Interpretation: D.J., B.B.P, K.N.H., C.E.H., V.Q., H.L., & J.O.
Writing: D.J., B.B.P., V.Q., H.L., J.O.
All authors reviewed and revised the manuscript.

Conflicts of Interest:

The authors declare no potential conflicts of interest.

Materials and Methods:

1. The mathematical model of metabolism

We utilize our previously developed mathematical model of metabolism (3,15) to analyze the emergence of the L/L phenotype. In brief, the generic form of the differential equation representing the temporal dynamics of x (pAMPK, HIF-1, mtROS or noxROS) is

$$dx/dt = g\_x*F\_g - k\_x*F\_k,$$

where g_x and k_x represent the basal production and degradation rates of x respectively. F_g and F_k represent the regulation of the production and degradation of x by others respectively. Considering the chemical reaction happens much faster relative to gene regulation, we assume the metabolic pathways reach an equilibrium state at certain levels of pAMPK and HIF-1. The

details of all equations can be found in the ***Supplementary Note***. The values of all parameters can be found in ***Supplementary Tables S2-3***.

2. The AMPK/HIF-1 signature

Since the active form of AMPK is pAMPK, the mRNA expression of AMPK is not indicative of AMPK activity (*23*). HIF-1 is often stabilized in cancer due to the commonly hypoxic condition faced by cancer cells. The mRNA expression of HIF-1 is also not indicative of HIF-1 activity. We quantify the AMPK and HIF-1 activity by evaluating the expression of their downstream targets respectively. We perform PCA of the gene expression data of AMPK and HIF-1 downstream targets respectively, from which we assign the PC1s as the signatures. The AMPK and HIF-1 downstream target genes can be found in ***Supplementary Table S4***.

3. The metabolic pathway scoring metric

We assume that higher activity of the metabolic process would need higher levels of enzymes which function in that process. Higher metabolic pathway scores indicate higher activity of the corresponding metabolic process. With this assumption, we quantify the activity of TCA, glycolysis and FAO by considering the expression of a total of 10 TCA enzyme genes, 8 glycolysis genes and 14 FAO enzyme genes. The full list of the enzyme genes can be found in ***Supplementary Table S5***. The genes used in the metabolic pathway scoring metric do not overlap with the genes used to construct the AMPK/HIF-1 signatures.

4. RNA-Seq of single-cell derived melanoma cells

RNA-Seq of melanoma cell lines (SKMEL5 subclones) was performed as previously reported (25). Briefly, RNA samples for each subclone, each in triplicate, were collected at three time points (day 0, day 3, and day 8) upon treatment with 8uM PLX4720. All downstream analyses were performed in R (https://www.r-project.org) using the Bioconductor framework (https://www.bioconductor.org). The expression data can be found in ***Supplementary Table S6***.

5. Seahorse metabolic assays

Seahorse metabolic assays to measure the oxygen consumption rate (OCR) and extracellular acidification rate (ECAR) were performed as previously reported (6). In brief, SKMEL5 subclones were treated with either DMSO or 8uM PLX4720 for 8 days and plated in 96-well plates (Seahorse Biosciences, Bilerica, MA) at a density of 25,000 cells 24 hours before analysis on the Seahorse XFe 96 extracellular flux analyzer. Mitochondrial oxygen consumption

was quantified using the Mito Stress Test kit, and the glycolytic rate was quantified using the Glycolysis Stress Test kit, each according to the manufacturers' instructions.

References:

1. Vander Heiden MG, Cantley LC, Thompson CB. Understanding the Warburg effect: the metabolic requirements of cell proliferation. Science. 2009;324:1029–33.

2. Porporato PE, Payen VL, Pérez-Escuredo J, De Saedeleer CJ, Danhier P, Copetti T, et al. A mitochondrial switch promotes tumor metastasis. Cell Rep. 2014;8:754–66.

3. Jia D, Lu M, Jung KH, Park JH, Yu L, Onuchic JN, et al. Elucidating cancer metabolic plasticity by coupling gene regulation with metabolic pathways. Proc Natl Acad Sci U S A. 2019;116:3909–18.

4. Haq R, Shoag J, Andreu-Perez P, Yokoyama S, Edelman H, Rowe GC, et al. Oncogenic BRAF regulates oxidative metabolism via PGC1α and MITF. Cancer Cell. 2013;23:302–15.

5. Baenke F, Chaneton B, Smith M, Van Den Broek N, Hogan K, Tang H, et al. Resistance to BRAF inhibitors induces glutamine dependency in melanoma cells. Mol Oncol. 2016;10:73–84.

6. Hardeman KN, Peng C, Paudel BB, Meyer CT, Luong T, Tyson DR, et al. Dependence On Glycolysis Sensitizes BRAF-mutated Melanomas For Increased Response To Targeted BRAF Inhibition. Sci Rep. 2017;7:42604.

7. Parmenter TJ, Kleinschmidt M, Kinross KM, Bond ST, Li J, Kaadige MR, et al. Response of BRAF-mutant melanoma to BRAF inhibition is mediated by a network of transcriptional regulators of glycolysis. Cancer Discov. 2014;4:423–33.

8. Viswanathan VS, Ryan MJ, Dhruv HD, Gill S, Eichhoff OM, Seashore-Ludlow B, et al. Dependency of a therapy-resistant state of cancer cells on a lipid peroxidase pathway. Nature. 2017;547:453–7.

9. Wood TK, Knabel SJ, Kwan BW. Bacterial Persister Cell Formation and Dormancy [Internet]. Applied and Environmental Microbiology. 2013. page 7116–21. Available from: http://dx.doi.org/10.1128/aem.02636-13

10. Sharma SV, Lee DY, Li B, Quinlan MP, Takahashi F, Maheswaran S, et al. A chromatin-mediated reversible drug-tolerant state in cancer cell subpopulations. Cell. 2010;141:69–80.

11. Collado M, Blasco MA, Serrano M. Cellular senescence in cancer and aging. Cell. 2007;130:223–33.

12. Aguirre-Ghiso JA. Models, mechanisms and clinical evidence for cancer dormancy. Nat Rev Cancer. 2007;7:834–46.

13. Ravindran Menon D, Das S, Krepler C, Vultur A, Rinner B, Schauer S, et al. A stress-induced early innate response causes multidrug tolerance in melanoma. Oncogene. 2015;34:4448–59.

14. Paudel BB, Harris LA, Hardeman KN, Abugable AA, Hayford CE, Tyson DR, et al. A Nonquiescent “Idling” Population State in Drug-Treated, BRAF-Mutated Melanoma. Biophys J. 2018;114:1499–511.

15. Yu L, Lu M, Jia D, Ma J, Ben-Jacob E, Levine H, et al. Modeling the Genetic Regulation of Cancer Metabolism: Interplay between Glycolysis and Oxidative Phosphorylation. Cancer Res. 2017;77:1564–74.

16. Eales KL, Hollinshead KER, Tennant DA. Hypoxia and metabolic adaptation of cancer cells. Oncogenesis. 2016;5:e190.

17. Huang B, Lu M, Jia D, Ben-Jacob E, Levine H, Onuchic JN. Interrogating the topological robustness of gene regulatory circuits by randomization. PLoS Comput Biol. 2017;13:e1005456.

18. Abildgaard C, Guldberg P. Molecular drivers of cellular metabolic reprogramming in melanoma. Trends Mol Med. 2015;21:164–71.

19. Tsoi J, Robert L, Paraiso K, Galvan C, Sheu KM, Lay J, et al. Multi-stage Differentiation Defines Melanoma Subtypes with Differential Vulnerability to Drug-Induced Iron-Dependent Oxidative Stress. Cancer Cell. 2018;33:890–904.e5.

20. Song C, Piva M, Sun L, Hong A, Moriceau G, Kong X. Recurrent tumor cell–intrinsic and–extrinsic alterations during MAPKi-induced melanoma regression and early adaptation. Cancer Discov [Internet]. AACR; 2017; Available from: http://cancerdiscovery.aacrjournals.org/content/7/11/1248.abstract

21. Hangauer MJ, Viswanathan VS, Ryan MJ, Bole D, Eaton JK, Matov A, et al. Drug-tolerant persister cancer cells are vulnerable to GPX4 inhibition. Nature. 2017;551:247–50.

22. Vazquez F, Lim J-H, Chim H, Bhalla K, Girnun G, Pierce K, et al. PGC1α expression defines a subset of human melanoma tumors with increased mitochondrial capacity and resistance to oxidative stress. Cancer Cell. 2013;23:287–301.

23. Cesi G, Walbrecq G, Zimmer A, Kreis S, Haan C. ROS production induced by BRAF inhibitor treatment rewires metabolic processes affecting cell growth of melanoma cells. Mol Cancer. 2017;16:102.

24. Smith MP, Brunton H, Rowling EJ, Ferguson J, Arozarena I, Miskolczi Z, et al. Inhibiting Drivers of Non-mutational Drug Tolerance Is a Salvage Strategy for Targeted Melanoma Therapy. Cancer Cell. 2016;29:270–84.

25. Meyer CT, Wooten DJ, Paudel BB, Bauer J, Hardeman KN, Westover D, et al. Quantifying Drug Combination Synergy along Potency and Efficacy Axes. Cell Syst. 2019;8:97–108.e16.

Figure Legends:

Figure 1. Modeling-predicted metabolically-inactive L/L phenotype in cancer. *(A)* Hierarchical clustering analysis (HCA) of the stable-state solutions from 500 sets of parameters. Each row represents one stable-state solution, referred to as one sample here. Each column represents the levels of a regulatory protein, a metabolite or the rate of one metabolic pathway. “F”

represents the FAO rate, "R_{mt}" represents the level of mtROS, "G_1" represents the glucose oxidation rate, "A" represents the level of pAMPK, R_{nox} represents the level of noxROS, "H" represents the level of HIF-1 and "G_2" represents the glycolysis rate. Different colors of the lineages correspond to different clusters. "O" corresponds to an OXPHOS phenotype. "W/O" corresponds to a hybrid metabolic phenotype. "L/L" corresponds to a low/low phenotype and "W" corresponds to a glycolysis phenotype. *(B)* PCA of the clustered samples in (A). Projection of the clustered sample in *A* to the pAMPK and HIF-1 axes *(C, top)*, to the $G_{1,\ ATP}$, $G_{2,\ ATP,}$ and F_{ATP} *axes(C, bottom)*. $G_{1,\ ATP}$, $G_{2,\ ATP,}$ and F_{ATP} represent the ATP production rates of glucose oxidation, glycolysis and FAO respectively. *(D)* Evaluating the effects of HIF-1α degradation and mtROS production on the fractions of different metabolic states. Two values of mtROS production rates 45 mM/min and 30 mM/min are used to simulate "high mtROS" and "low mtROS" respectively. Two values of HIF-1 degradation rates 0.25 h^{-1} and 0.45 h^{-1} are used to simulate "high HIF-1" and "low HIF-1" respectively. 500 sets of parameters were used to collect the stable-state solutions for each scenario. The solutions of each scenario were first normalized using the mean and standard deviation (std) calculated in the scenario (high mtROS, high HIF-1), clustered and projected onto the PC1 and PC2 generated by the scenario (high mtROS, high HIF-1). *(E)* The fractions of the L/L phenotype corresponding to each scenario in *D*. The analysis was repeated for three times and error bars were added. The color codes for different metabolic states "W", "O", "W/O" and "L/L" are consistent in figures *B-D*.

Figure 2. Melanoma cells entering an idling state exhibit the L/L feature. (*A*) Growth rate of three single-cell-derived SKMEL5 subclones, SC01, SC07 and SC10 in either *early* (untreated) condition or in the *Idling* state (8 days in 8uM PLX4720). (*B*) The mean AMPK and HIF-1 signatures of each subclone at indicated time points. (*C*) Box plots for the TCA score, FAO score and glycolysis score of SC01, SC07, and SC10. For SC01: TCA score, $P_{basal\text{-}day3}$=0.04; FAO score, $P_{day3\text{-}day8}$=0.03; glycolysis score, $P_{basal\text{-}day8}$=0.01, $P_{day3\text{-}day8}$=0.02. For SC10: TCA score, $P_{basal\text{-}day3}$=0.003, $P_{day3\text{-}day8}$<0.0001; FAO score, $P_{basal\text{-}day3}$=0.009, $P_{day3\text{-}day8}$=0.004; glycolysis score, $P_{basal\text{-}day8}$=0.01, $P_{day3\text{-}day8}$<0.0009. (*D*) OCR (top panel) and ECAR (bottom panel) of three SC01, SC07, and SC10 in either their *basal* (untreated) conditions or in *Idling* state (8 days in 8uM PLX4720), error bars mean ± SEM. (*E*) Heat-map of metabolic parameters for three subclones in *basal* vs *idling* state extracted from Seahorse assays in Fig. 2D - the first four parameters from a glycolytic function experiment (Glyco Stress Test) and the second four parameters from a mitochondria function experiment (Mito Stress Test). (*F*) Aggregated glycolytic parameters plotted against aggregated OXPHOS parameters for three subclones in *basal* vs *idling* state, arrows show the direction of change in idling state from their basal counterparts. (*G*) First two principal components from the time-course RNA-Seq data on genes involved in metabolism in three subclones, SC01, SC07, and SC10 in control, 3 days and 8 days in 8uM PLX4720, arrows indicate the shift in transcriptome of subclones along PC1 and PC2 axes.

Figure 3. Residual melanoma tumors upon MAPKi therapy exhibit L/L signature. The AMPK/HIF-1 signatures and TCA/glycolysis scores of BRAF-mutated tumor samples upon MAPKi treatment for the indicated time points. The RNA-Seq data are obtained from GEO with

the series ID GSE75299. The red arrows denote the direction of the change of AMPK and HIF-1 activity of samples upon MAPKi treatment.

Figures

Figure 1

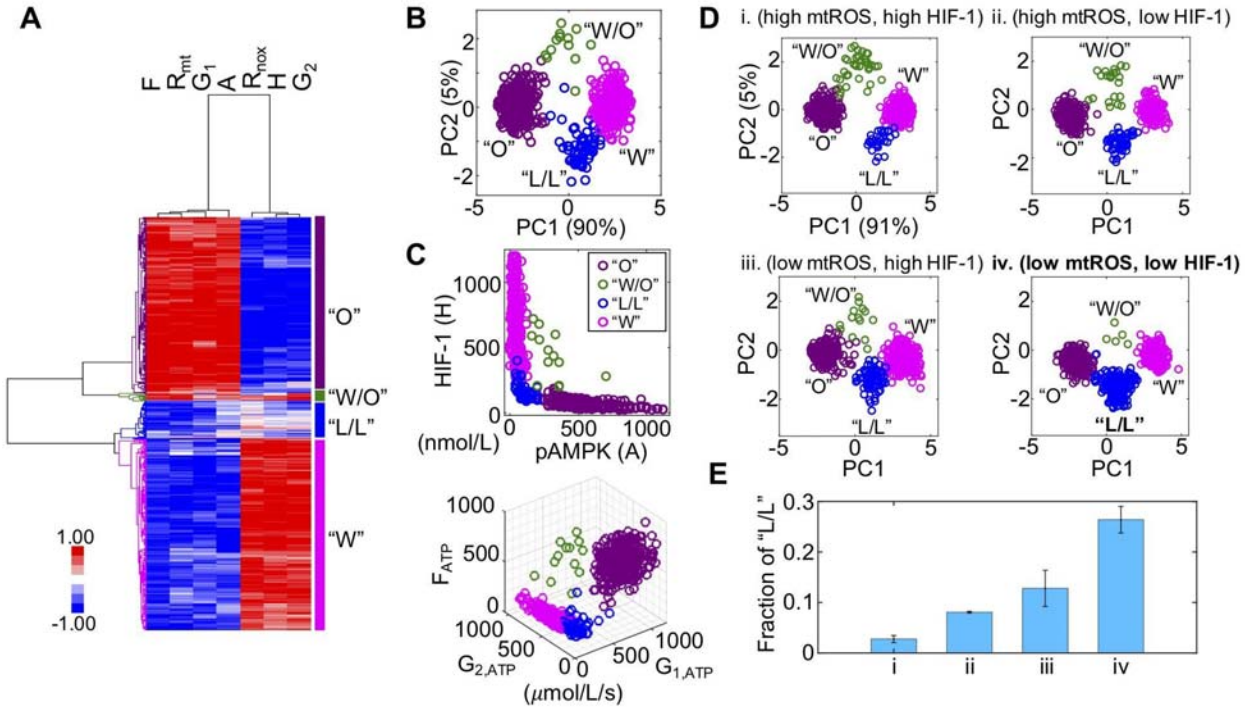

Figure 2

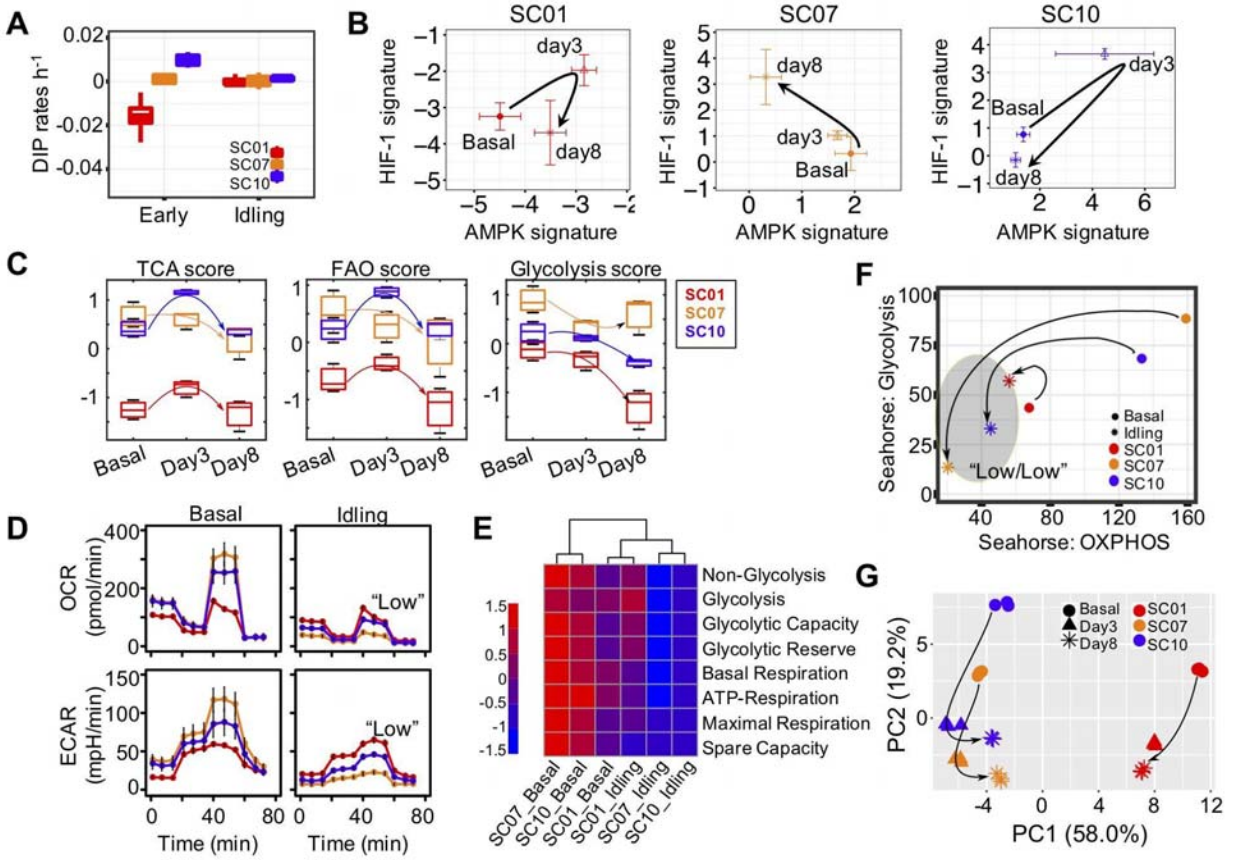

Figure 3